

Conceptually new mechanism for trapping neutral, polar particles.

R. Blümel

Department of Physics, Wesleyan University, Middletown, Connecticut 06459-0155

(Dated: June 27, 2022)

It is shown that a superposition of static and rapidly oscillating electric *monopole* (source) fields is capable of trapping particles with a permanent electric dipole moment. Thus, the new trapping mechanism differs fundamentally from saddle-point traps that use static and oscillating higher-multipole fields. An analytical stability analysis together with detailed molecular dynamics trajectory calculations prove that the trap is stable. Thin rods of barium titanate (BaTiO_3) provide an illustrative example for the working principle of the new trap. The effects of gravity are considered. The existence of a bifurcation regime is predicted. A particular strength of the new trap is that it also works for zero orbital angular momentum with respect to the field-generating electrodes.

PACS numbers: 37.10.Pq, 77.22.-d

I. INTRODUCTION

Levitation of microscopic and macroscopic objects is of general interest in physics: It is a key technology for basic and applied sciences. For instance, research areas ranging from high-resolution spectroscopy [1–3], frequency standards [4], neutral anti-matter production [5, 6], Bose-Einstein condensation [7, 8], and quantum computing [9] to high-speed trains [10], all rely on the levitation and three-dimensional confinement of objects by electromagnetic fields. The key point is that electromagnetic confinement provides “walls of pure energy” that avoid contamination, friction, and, in the case of antimatter, annihilation, by avoiding contact with material walls.

Traps used in science and technology may broadly be divided into charged-particle traps and neutral-particle traps. Historically, charged-particle traps were developed first, starting with the development of the Kingdon trap [11] in the 1920s, the Penning trap [12] in the 1930s and the Paul trap [13] in the 1950s. In addition to their use in high-resolution spectroscopy [1–3], frequency standards [4], and quantum computing [9], these traps were used, e.g., as a model for planetary dynamics [14], for studying collisions and excited-state lifetimes of ions [15], and the production and investigation of Coulomb crystals [16–18]. Recently, neutral-particle traps were developed and demonstrated as well. Based on the type of field employed, we may distinguish several different types of neutral-particle traps, for instance, electric [19–25], magnetic [26, 27], or light-field traps [28, 29].

The purpose of this paper is to introduce a conceptually new trap for the stable confinement of neutral, polar particles. The trapping mechanism of the new trap is fundamentally different from the trapping mechanisms employed in existing neutral-particle traps: (i) The trap does not make use of energy shifts in selected quantum states and (ii) in contrast to existing traps [23, 24], which are based on a dynamic saddle-point potential akin to the strong-focusing Paul-trap principle [13], the new trap works on the basis of a superposition of static and oscillating *monopole* fields.

The paper is organized in the following way. In Sec. II we derive the coupled radial and angular equations of motion of point dipoles trapped in a combination of ac and dc electric monopole (source) fields. In Sec. III we analyze the stability of the coupled system of equations and derive conditions for the stable confinement of point dipoles. We conclude that stable trapping is possible as long as stable solutions of the radial equation exist. Therefore, in Sec. IV, we investigate in detail the stability properties of the radial equation. We find that subject to certain conditions on the control parameter of the radial equation, the radial equation is stable, which guarantees the stability of the combined radial and angular system of equations derived in Sec. II, and thus results in stable confinement of point dipoles according to the new trapping scheme. In Sec. V, strengthening our analytical results, we show numerically that the trap is stable. In Sec. VI we derive the conditions under which stable confinement in the presence of gravity is achieved. In Sec. VII we state a step-by-step algorithm according to which trap parameters may be designed. The trapping of thin, cylindrical rods of barium titanate is discussed in Sec. VIII. In Sec. IX we discuss our results. In Sec. X we summarize our results and conclude the paper.

II. EQUATIONS OF MOTION

In this section we derive the equations of motion of a point dipole \mathbf{p} of mass M and moment of inertia I in an electric field

$$\mathbf{E}(r, t) = \frac{\nu V(t)}{r^\alpha} \hat{\mathbf{r}}, \quad (1)$$

where $\nu > 0$ and $\alpha > 0$ are constants, r is the distance of the dipole from the source of the field, $\hat{\mathbf{r}}$ is the unit vector in \mathbf{r} direction, and $V(t)$ is the voltage applied to the electrodes that generate the field \mathbf{E} . Since the interaction energy of a point dipole \mathbf{p} with an electric field \mathbf{E} is

$$W = -\mathbf{p} \cdot \mathbf{E} = -pE \cos(\theta), \quad (2)$$

where θ is the angle between \mathbf{p} and \mathbf{E} , the Lagrangian function \mathcal{L} of the point dipole in the case of zero orbital angular momentum is

$$\mathcal{L} = \frac{1}{2}M\dot{r}^2 + \frac{1}{2}I[\dot{\theta}^2 + \sin^2(\theta)\dot{\varphi}^2] + \frac{p\nu V(t)}{r^\alpha} \cos(\theta), \quad (3)$$

where φ is the azimuthal angle of \mathbf{p} . Since $\partial\mathcal{L}/\partial\varphi = 0$, the azimuthal angle is a cyclic variable [30], and the conjugate canonical momentum,

$$L_\varphi = \frac{\partial\mathcal{L}}{\partial\dot{\varphi}} = I \sin^2(\theta)\dot{\varphi}, \quad (4)$$

is a constant of the motion. In the following we specialize to the case $L_\varphi = 0$. While some neutral-particle traps require non-zero orbital angular momentum to work properly (an example is the trap described in [20, 21]), a particular strength of the trap introduced in this paper is that it works for zero orbital angular momentum. Therefore, playing to the strength of the new trap, we treat the case in which the dipole is not rotating around the field source, i.e. the orbital angular momentum of the point dipole around the field-generating electrodes is zero. It has been checked by means of extensive numerical simulations that the trap also works for non-zero orbital angular momentum. However, since this case does not add substantial additional insight into the fundamental working principle of the new trap, the case of non-zero orbital angular momentum is not treated in this paper and we will continue to focus on the case of zero orbital angular momentum as reflected in the Lagrangian function (3). On the basis of the Lagrangian function (3) the radial (r) and angular (θ) equations of motion are obtained from the Lagrangian equations [30]

$$\frac{d}{dt} \frac{\partial\mathcal{L}}{\partial\dot{r}} - \frac{\partial\mathcal{L}}{\partial r} = 0, \quad \frac{d}{dt} \frac{\partial\mathcal{L}}{\partial\dot{\theta}} - \frac{\partial\mathcal{L}}{\partial\theta} = 0. \quad (5)$$

From (3) with (5) we obtain

$$\ddot{r} + \frac{p\alpha\nu V(t) \cos(\theta)}{Mr^{\alpha+1}} = 0, \quad (6)$$

$$\ddot{\theta} + \frac{p\nu V(t) \sin(\theta)}{Ir^\alpha} = 0. \quad (7)$$

We now specialize the voltage $V(t)$ to

$$V(t) = V_{\text{dc}} - V_{\text{ac}} \cos(\Omega t), \quad (8)$$

where $V_{\text{dc}} > 0$ is the dc part of the voltage, $V_{\text{ac}} > 0$ is the ac part of the voltage, and Ω is the angular frequency of the ac part of the voltage. We also define the dimensionless control parameters

$$\eta = \frac{V_{\text{ac}}}{2V_{\text{dc}}} \quad (9)$$

and

$$\beta = \frac{Ml_0^2}{\alpha I}, \quad (10)$$

the unit of time

$$t_0 = \frac{2}{\Omega} \quad (11)$$

and the unit of length

$$l_0 = \left(\frac{4\alpha p\nu V_{\text{dc}}}{M\Omega^2} \right)^{\frac{1}{\alpha+2}}, \quad (12)$$

such that

$$\rho = \frac{r}{l_0} \quad (13)$$

and

$$\tau = \frac{t}{t_0} \quad (14)$$

are the dimensionless radius and time, respectively. In terms of ρ and τ , with (9) – (14), the dimensionless equivalents of (6) and (7) are

$$\ddot{\rho} + [1 - 2\eta \cos(2\tau)] \frac{\cos(\theta)}{\rho^{\alpha+1}} = 0, \quad (15)$$

$$\ddot{\theta} + \beta[1 - 2\eta \cos(2\tau)] \frac{\sin(\theta)}{\rho^\alpha} = 0, \quad (16)$$

where the dots now indicate differentiation with respect to τ .

III. LINEAR STABILITY ANALYSIS

It is not obvious that the equations of motion (15) and (16) have stable solutions. Indeed, we will see in this and following sections, that both η and β need to satisfy certain conditions in order for (15) and (16) to exhibit stable solutions. To find the condition for β , we perform a linear stability analysis. We emphasize that expanding the equations of motion to linear order is not an uncontrolled approximation. In the absence of pathologies – as is the case here – it is an exact method for assessing the stability properties of the equilibrium solution of the equations of motion [31].

To first order in θ , we may replace $\cos(\theta)$ by 1 to obtain

$$\ddot{\rho} + [1 - 2\eta \cos(2\tau)] \frac{1}{\rho^{\alpha+1}} = 0. \quad (17)$$

Thus, to linear order, the ρ equation decouples from the θ equation. This fact substantially simplifies the stability analysis. However, the θ equation remains coupled to the ρ equation since even in linear order the θ equation contains ρ . To lowest order the Fourier expansion of the exact solution $\rho(\tau)$ of (17) is given by

$$\rho(\tau) = \rho_0 - \rho_1 \cos(2\tau), \quad (18)$$

where ρ_0 and ρ_1 are constants. Inserting (18) into (17), replacing $\cos^2(2\tau)$ terms by their average value $1/2$, and neglecting $(\alpha + 1)\rho_1/\rho_0$ with respect to 2η , the ρ equation (17) is fulfilled if

$$\rho_0 = \left(\frac{\alpha + 1}{2} \right)^{\frac{1}{\alpha+2}} \eta^{\frac{2}{\alpha+2}}, \quad (19)$$

$$\rho_1 = \left[2^{\frac{1}{\alpha+2}} (\alpha + 1)^{\frac{\alpha+1}{\alpha+2}} \eta^{\frac{\alpha}{\alpha+2}} \right]^{-1}. \quad (20)$$

Inserting (18) into (16), keeping only terms linear in ρ_1 , and replacing once more all $\cos^2(2\tau)$ terms by $1/2$, we obtain

$$\ddot{\theta} + \frac{\beta}{\rho_0^\alpha} \left\{ \left(\frac{1}{\alpha + 1} \right) - 2\eta \left[1 - \frac{\alpha}{2\eta^2(\alpha + 1)} \right] \cos(2\tau) \right\} \sin(\theta) = 0. \quad (21)$$

Furthermore, since we are focusing on small oscillations, we may safely replace $\sin(\theta)$ by θ . In addition, as we will see below, η is usually quite large ($\eta \gtrsim 10$) so that we may neglect the term $\alpha/[2\eta^2(\alpha + 1)]$ with respect to 1. Together, this yields

$$\ddot{\theta} + \frac{\beta}{\rho_0^\alpha} \left[\left(\frac{1}{\alpha + 1} \right) - 2\eta \cos(2\tau) \right] \theta = 0. \quad (22)$$

This is a Mathieu equation [32], whose canonical form is [32]

$$\ddot{x} + [a - 2q \cos(2\tau)] x = 0. \quad (23)$$

Comparing (23) with (22) we see that

$$a = \frac{\beta}{(\alpha + 1)\rho_0^\alpha}, \quad (24)$$

$$q = \frac{\beta\eta}{\rho_0^\alpha}. \quad (25)$$

It is well known [32] that stable solutions of (23) exist only in certain two-dimensional regions of the (q, a) parameter plane [32]. Because of $\rho_0 > 0$ and the definitions of α and β in (1) and (10), respectively, we have $a > 0$. In this case, and up to second order in q , the first, and most important, stability region of the Mathieu equation is bounded by [32]

$$0 < a < 1 - q - \frac{q^2}{8}. \quad (26)$$

With (24) and (25) we have

$$a = \frac{q}{(\alpha + 1)\eta}. \quad (27)$$

Using this in (26), we obtain the following quadratic inequality for q :

$$q^2 + 8q \left[1 + \frac{1}{(\alpha + 1)\eta} \right] - 8 < 0. \quad (28)$$

Keeping only terms up to first order in $1/[(\alpha + 1)\eta]$, the solution is

$$q < q_s(\eta), \quad (29)$$

where

$$q_s(\eta) = (-4 + 2\sqrt{6}) - \frac{4}{(\alpha + 1)\eta} \left[1 - \frac{\sqrt{6}}{3} \right] \quad (30)$$

$$= 0.9 - \frac{0.734}{(\alpha + 1)\eta}. \quad (31)$$

With (19) and (25) this yields the stability criterion

$$\beta < q_s(\eta) \frac{\rho_0^\alpha}{\eta} = q_s(\eta) \left(\frac{\alpha + 1}{2} \right)^{\frac{\alpha}{\alpha+2}} \eta^{\frac{\alpha-2}{\alpha+2}}. \quad (32)$$

In summary, a range of β values exists that leads to stable θ oscillations. This result is significant. It means that as long as stable solutions of (17) exist, stable solutions of the system (15) and (16) can be constructed, which, in turn, implies stable confinement of dipoles. Therefore, before proceeding further, we need to investigate the stability properties of the radial equation (17).

IV. PROPERTIES OF THE RADIAL EQUATION

A pseudo-potential analysis [33] is the most natural way to conduct a comprehensive stability analysis of the radial equation (17). It is a powerful method that may be applied generally for the analysis of the motion of particles in rapidly oscillating force fields [30]. According to this method, we start with (18), but instead of holding ρ_0 fixed, we allow $\rho(\tau)$ to execute slow oscillations around ρ_0 . Therefore, we now write

$$\rho(\tau) = R(\tau) - \rho_1 \cos(2\tau), \quad (33)$$

where, as in (18), ρ_1 is a constant. Equation (33) represents formally what actually happens physically: The exact motion $\rho(\tau)$ is a superposition of a slow, large-amplitude motion $R(\tau)$ and a fast, small-amplitude motion proportional to $\cos(2\tau)$ [30]. The slow, large-amplitude motion is known as the macro-motion; the fast, small-amplitude motion

is the micro-motion. Apparently, because it determines the cycle-averaged trajectory of a trapped particle, it is the behavior of $R(\tau)$, which determines the stability properties of the trap.

Inserting (33) into (17), keeping only terms up to first order in ρ_1 , and, as we did before, replacing $\cos^2(2\tau)$ by its average value $1/2$, we obtain

$$\left[\ddot{R} + \frac{1}{R^{\alpha+1}} - \frac{\eta(\alpha+1)\rho_1}{R^{\alpha+2}} \right] + \left\{ 4\rho_1 - \frac{1}{R^{\alpha+1}} \left[2\eta - (\alpha+1)\frac{\rho_1}{R} \right] \right\} \cos(2\tau) = 0. \quad (34)$$

This equation is fulfilled if, separately,

$$\ddot{R} + \frac{1}{R^{\alpha+1}} - \frac{\eta(\alpha+1)\rho_1}{R^{\alpha+2}} = 0, \quad (35)$$

$$4\rho_1 - \frac{1}{R^{\alpha+1}} \left[2\eta - (\alpha+1)\frac{\rho_1}{R} \right] = 0. \quad (36)$$

Neglecting the term $(\alpha+1)\rho_1/R$ in (36) with respect to 2η , equation (36) yields

$$\rho_1 = \frac{\eta}{2R^{\alpha+1}}. \quad (37)$$

Inserting this result into (35) yields

$$\ddot{R} = -\frac{1}{R^{\alpha+1}} + \frac{(\alpha+1)\eta^2}{2R^{2\alpha+3}} = -\frac{\partial V_{\text{eff}}(R)}{\partial R}, \quad (38)$$

where

$$V_{\text{eff}}(R) = -\frac{1}{\alpha R^\alpha} + \frac{\eta^2}{4R^{2\alpha+2}} \quad (39)$$

is known as the effective potential [30], the pseudo-potential [33], or the ponderomotive potential in atomic [34] and plasma [35] physics. Apparently, the motion of the point dipole, on average, behaves as if the dipole were under the influence of a force that is the gradient of the pseudo-potential $V_{\text{eff}}(R)$. This is a powerful result that allows us to determine the stability of the motion of the point dipole according to physical reasoning: If $V_{\text{eff}}(R)$ has a potential minimum, the point dipole will execute stable, oscillatory motion inside of the potential minimum; the point dipole is trapped. If V_{eff} does not have a potential minimum, the point dipole will escape to infinity, and no stable trapping is observed. A potential minimum occurs at points R_0 for which $V'_{\text{eff}}(R_0) = 0$ and $V''_{\text{eff}}(R_0) > 0$. Indeed, $V'_{\text{eff}}(R_0) = 0$ has a single solution for

$$R_0 = \rho_0, \quad (40)$$

where ρ_0 is defined in (19). Apparently, linear stability analysis and pseudo-potential analysis are consistent in that they predict the same equilibrium radius ρ_0 . Moreover, we have

$$V''_{\text{eff}}(R_0) = \frac{2(\alpha+2)}{(\alpha+1)\eta^2} > 0, \quad (41)$$

i.e., $R_0 = \rho_0$, in fact, corresponds to a pseudo-potential minimum for all control parameters η . At this point we have to remember that in our pseudo-potential analysis we neglected higher-order terms in ρ_1/R . Thus, we expect the pseudo-potential analysis to be trustworthy only for $\rho_1/R_0 \ll 1$, which implies

$$\eta \gg \frac{1}{\alpha+1}. \quad (42)$$

Physically, the condition $\rho_1/R_0 \ll 1$, or, equivalently, $R_0 \gg \rho_1$ means that the amplitude ρ_1 of the fast oscillations around R_0 needs to be small enough with respect to R_0 such that the dipole does not hit the field-generating source at $r = 0$. This, however, would indeed occur for $R_0 < \rho_1$ and lead to the ejection of the point dipole from the trap. Indeed, there is “trouble” for small η . It is known [36] that for $\alpha = 0$ the radial equation (17) exhibits a period-doubling bifurcation at $\eta_1 \approx 3.12$ and further period-doubling bifurcations, following the Feigenbaum scenario [31], at $\eta_{j+1} < \eta_j$, $j = 1, 2, \dots$, terminating in a transition to fully developed chaos at $\eta_\infty \approx 2.91$. This means that

in $\eta_{j+1} < \eta < \eta_j$, $j = 1, 2, \dots$, the lowest Fourier component of $\rho(\tau)$ is not $\cos(2\tau)$, as in (18), but $\cos(2\tau/2^j)$. This is not taken into account in (18). As a consequence, our pseudo-potential analysis is not valid for $\eta < \eta_1$. Detailed calculations show that (i) the period-doubling scenario persists for $\alpha > 0$, and (ii) that $\eta_1(\alpha)$ is a slowly, monotonically decreasing function of α , ranging from $\eta_1(\alpha = 0) \approx 3.12$ to $\eta_1(\alpha = 10) \approx 2.41$. It is important to emphasize that the occurrence of bifurcations does not preclude stable trapping. Indeed, stable trapping, in principle, may be achieved in the entire range $[\eta_\infty < \eta < \eta_1]$. Thus, the existence and location of the predicted bifurcations may be explored experimentally. However, since in this region, as mentioned above, the point dipole is already very close to the field-generating source(s), it may be very difficult to trap dipoles experimentally in the bifurcation regime.

Another source of trouble for the pseudo-potential analysis are resonances, which occur for $\eta > \eta_1$. Resonances occur whenever the frequency of oscillations in the pseudo-potential well V_{eff} is a rational multiple of the driving frequency of the trap. Luckily, only the lowest order resonances are “dangerous”. They occur whenever the low-frequency oscillations of $R(\tau)$ in (33) are $1/3$ or $1/2$ of the driving frequency ($= 2$) in (17). Although the pseudo-potential analysis, incorrectly, predicts stability in these resonant cases, it is not entirely useless. Since $\eta > \eta_1$, the conditions for the computation of the pseudo-potential are met. Therefore, there is nothing wrong with computing the frequency of slow oscillations of the dipole in the pseudo-potential V_{eff} and, on the basis of this result, to predict the η values at which the resonant instabilities occur. Since the frequency ω of small oscillations around the equilibrium radius ρ_0 is

$$\omega = \sqrt{V''_{\text{eff}}(\rho_0)}, \quad (43)$$

the instability at $\omega = 2/3$ is predicted to occur at

$$\eta_3^* = \frac{3}{2} \sqrt{\frac{2(\alpha + 2)}{\alpha + 1}}, \quad (44)$$

and the instability at $\omega = 1/2$ is predicted to occur at

$$\eta_4^* = 2 \sqrt{\frac{2(\alpha + 2)}{\alpha + 1}}, \quad (45)$$

where we used the expression (41) for $V''_{\text{eff}}(\rho_0)$. For $\alpha = 1$, we predict $\eta_3^* = 3\sqrt{3}/2 \approx 2.6$ and $\eta_4^* = 2\sqrt{3} \approx 3.5$ in fair agreement with the numerically obtained values $\eta_3^* \approx 3.16$ and $\eta_4^* \approx 3.86$, respectively [37]. More important than the numerical proximity of these special values is their behavior as a function of α . Equations (44) and (45) show that both η_3^* and η_4^* are bounded and never exceed $\eta = 4$.

Summarizing the results of this and the previous section, we obtain the following general result: In the absence of gravity, stable trapping of point dipoles may be achieved for all $\eta > 5$. Even for $\eta < 5$, ranges of η values exist for which stable trapping is possible. The $\eta < 5$ regime exhibits rich dynamics, but is less accessible to analytical analysis.

V. NUMERICAL INVESTIGATION OF STABILITY

In this section we back up the analytical calculations with numerical simulations. We solved the system of equations (15) and (16) numerically for $\eta = 100$, $\beta = 0.59$, and $\alpha = 2$ for the following 5929 initial conditions: $\rho(\tau = 0) = 13 + j \times 0.2$, $j = -5, \dots, 5$, $\dot{\rho}(\tau = 0) = k \times 0.01$, $k = -3, \dots, 3$, $\theta(\tau = 0) = l \times 0.03$, $l = -5, \dots, 5$, $\dot{\theta}(\tau = 0) = m \times 0.003$, $m = -3, \dots, 3$. Since the solutions of the system of equations (15) and (16) are well behaved, no special numerical integrator needs to be chosen. We chose a simple 4th order Runge-Kutta integrator [32], which yields completely converged, numerically exact solutions for any prescribed accuracy (we achieved a relative accuracy of better than 10^{-6} in all dynamical variables). Using the Runge-Kutta integrator, each of the 5929 initial conditions was propagated forward in time, and for each trajectory it was verified graphically that it stayed bounded over a time interval $\Delta\tau = 500\pi$.

A representative molecular trajectory is illustrated in Figs. 1 and 2. The trajectory picked is the one with initial conditions $\rho(0) = 13$, $\dot{\rho}(0) = 0$, $\theta(0) = 0.01$, and $\dot{\theta}(0) = 0$. Figure 1 (a) shows the time-evolution of $\rho(\tau)$ over the time interval $0 \leq \tau \leq 500\pi$. During this time interval, the macro-motion performs about three and a half oscillations, ranging between $\rho_{\min} = 9.8$ and $\rho_{\max} = 13$. Thus, the oscillations are bounded in the ρ direction. It is important to notice that the micro-motion is very small. In fact, the micro-motion amplitude is so small that it is not resolved on the scale of Fig. 1 (a) and manifests itself as a fine blur of the line. This is an important consistency check, since the pseudo-potential method is valid only if the micro-motion amplitude is small compared to the oscillations of the macro-motion. This is clearly born out in Fig. 1 (a). Since η is large, the small amplitude of the micro-motion observed in Fig. 1 (a) is consistent with its analytical prediction (20).

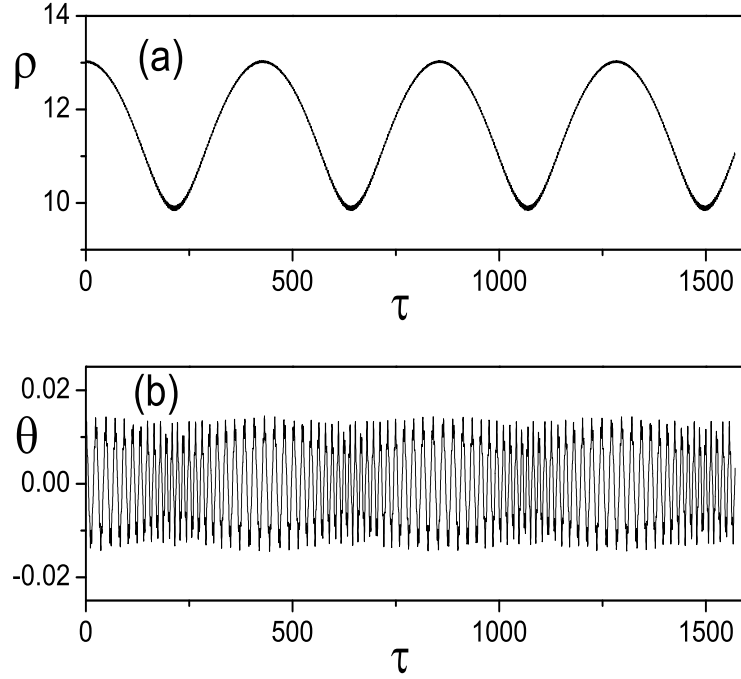


FIG. 1: Molecular trajectory calculation of (a) $\rho(\tau)$ and (b) $\theta(\tau)$ for initial conditions $\rho(0) = 13$, $\dot{\rho}(0) = 0$, $\theta(0) = 0.01$, and $\dot{\theta}(0) = 0$. The blurring of the line in (a) results from the micro-motion, which is not resolved on the scale of (a), and, as (a) shows, is very small. Panel (b) shows bounded oscillations of θ as a function of time. Together, (a) and (b) illustrate the stability of the trap. The calculations are numerically exact (converged) solutions of the equations of motion (15) and (16). No approximations were performed.

Figure 2 illustrates the stability of the representative molecular trajectory in phase space. This is a more stringent test of stability than the $\rho(\tau)$ and $\theta(\tau)$ trajectories displayed in Fig. 1, since the trajectory, e.g., might be stable in ρ , but unstable in $\dot{\rho}$. We show the molecular trajectory over the same time interval chosen in Fig. 1, i.e. $\Delta\tau = 500\pi$. Since the molecular trajectory is embedded in a 4-dimensional phase space ($\rho(\tau), \dot{\rho}(\tau), \theta(\tau), \dot{\theta}(\tau)$), we use the technique of Poincaré sections [31] to display the trajectory via six panels of two-dimensional phase-space projections. We choose the projections on the six possible two-dimensional coordinate planes (a) $\dot{\rho}$ vs. ρ , (b) θ vs. ρ , (c) $\dot{\theta}$ vs. ρ , (d) θ vs. $\dot{\rho}$, (e) $\dot{\theta}$ vs. $\dot{\rho}$, (f) $\dot{\theta}$ vs. θ . While the micro-motion is essential for generating the trapping forces, it is the macro-motion that determines the stability of the trap (see Sec. IV). Therefore, suppressing the irrelevant micro-motion and focusing on the relevant macro-motion, we strobe the motion, i.e., we display the trajectory at the end of each cycle of the trap field at the discrete times $\tau_j = j \times \pi$, $j = 1, \dots, 500$ (plot symbols in Fig. 2). Figure 2 (a) shows clearly that the trajectory executes a stable oscillation in ρ direction. Figure 2 (b) shows that the motion is also bounded in the ρ - θ plane. Figure 2 (c) shows new information; we see that the motion is also bounded in $\dot{\theta}$ direction. Figures 2 (d) and (e) contain the new information that the motion is also bounded in $\dot{\rho}$. Figure 2 (f) shows that the trajectory executes stable oscillations in the θ direction. The six panels taken together imply that there is no “escape direction” in phase space, i.e. the motion is globally stable. Plots akin to Figs. 1 and 2 were produced for each of the 5929 initial conditions and overlaid one of top of the other. The resulting composite plots look qualitatively like Figs. 1 and 2, showing no data points outside a confined area. This way it is possible to summarily assess stability of all 5929 molecular trajectories, without having to inspect them one-by-one individually. The net result is a numerical confirmation of stability of the trap in an entire four-dimensional phase-space volume.

Comparing Fig. 1 (b) with Figs. 2 (b), (d), and (f), one might perceive a problem: The θ amplitude in Fig. 1 (b) is larger than the θ spread in Figs. 2 (b), (d), and (f). The reason for this, however, is straightforward. It was checked explicitly that the reduction of spread in Figs. 2 (b), (d), and (f) is due to the strobing of the motion at multiples of π . Strobing does not display the motion over a continuous time interval, but samples the motion at discrete times.

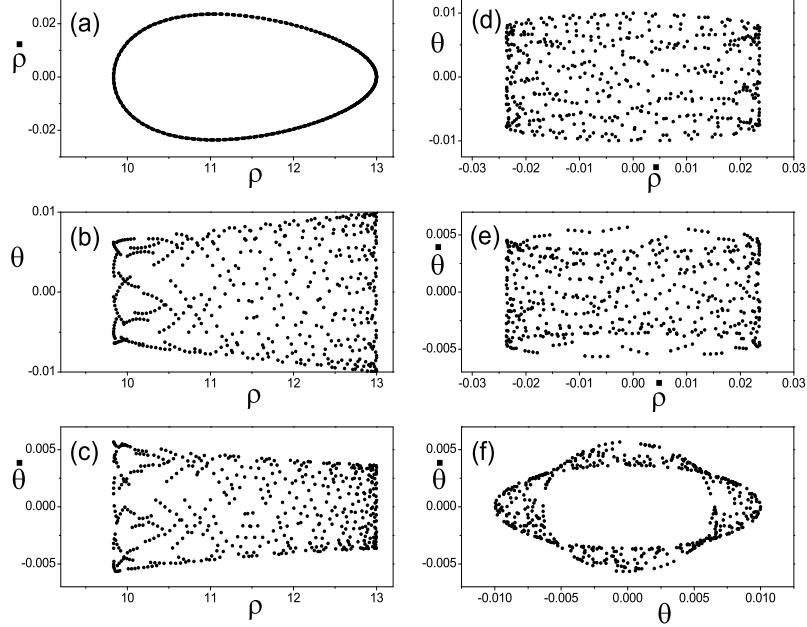


FIG. 2: Six stroboscopic sections of the 4-dimensional phase space of the molecular-dynamics trajectory of Fig. 1 for 500 cycles of the trap field. Each point in the figure represents the respective values of the trajectory at the end of each cycle. (a) $\dot{\rho}$ vs. ρ , (b) θ vs. ρ , (c) $\dot{\theta}$ vs. ρ , (d) θ vs. $\dot{\rho}$, (e) $\dot{\theta}$ vs. $\dot{\rho}$, (f) $\dot{\theta}$ vs. θ . The six sections show clearly that (i) the molecular trajectory is bounded in all four phase-space dimensions, and (ii) executes bounded oscillations in both ρ and θ directions.

This explains the small reduction in spread.

The numerical check performed amounts to a stability survey of a four-dimensional phase-space volume surrounding the point $(\rho(\tau = 0), \dot{\rho}(\tau = 0), \theta(\tau = 0), \dot{\theta}(\tau = 0))$ with a resolution of 5929 initial conditions that all lead to stable solutions of the system of equations (15) and (16). The composite phase-space plot produced by overlaying all 5929 individual phase-space plots reveals stable radial oscillations in the ρ interval $9 < \rho < 19$ and the θ interval $-0.3 < \theta < 0.3$.

Since dipole forces are usually much smaller than corresponding forces on isolated electric charges, we anticipate that consideration and inclusion of gravitational forces may be important for a proper description of the dynamics of trapped dipoles according to the new trapping scheme. We will address the influence of gravity next.

VI. BEATING GRAVITY

In previous sections we established that, in the absence of gravity, control parameter combinations (η, β) exist that result in the stable, permanent confinement of point dipoles. Since in this paper we are focusing on electric fields of the form (1), which vanish for large r , it is obvious that in certain trapping regimes gravity may overwhelm the confining effect of the electric field and result in a destabilization of the trap. Therefore, in this section, we study the effects of gravity and state the conditions that result in stable trapping in the presence of gravity.

In SI units, and according to (39), the pseudo-potential $V_{\text{eff}}(r)$ is given by

$$V_{\text{eff}}(r) = \left(\frac{M l_0^2}{t_0^2} \right) \left[-\frac{1}{\alpha \rho^\alpha} + \frac{\eta^2}{4 \rho^{2\alpha+2}} \right], \quad (46)$$

where $\rho = r/l_0$ is defined in (13). In the presence of gravity, $V_{\text{eff}}(r)$ is modified to $V_{\text{eff}}(r) \rightarrow V_{\text{eff}}(r) - Mgr$, i.e.

$$V_{\text{eff}}(r) = \left(\frac{M l_0^2}{t_0^2} \right) V_{\text{eff}}(\rho), \quad (47)$$

where

$$V_{\text{eff}}(\rho) = -\frac{1}{\alpha\rho^\alpha} + \frac{\eta^2}{4\rho^{2\alpha+2}} - \gamma\rho \quad (48)$$

with

$$\gamma = \frac{gt_0^2}{l_0}. \quad (49)$$

For stable trapping to occur, $V_{\text{eff}}(\rho)$ needs to exhibit a potential minimum, i.e. we require

$$V'_{\text{eff}}(\rho) = f(\rho) - \gamma = 0, \quad (50)$$

where

$$f(\rho) = \frac{1}{\rho^{\alpha+1}} - \frac{(\alpha+1)\eta^2}{2\rho^{2\alpha+3}}. \quad (51)$$

Since $\gamma > 0$, equation (50) has a solution only if the maximum of $f(\rho)$ exceeds γ . From $f'(\rho) = 0$ we determine that the maximum of $f(\rho)$ occurs at

$$\rho_{\text{max}} = \left(\frac{2\alpha+3}{2}\right)^{\frac{1}{\alpha+2}} \eta^{\frac{2}{\alpha+2}}, \quad (52)$$

which results in the minimum condition

$$\gamma < f(\rho_{\text{max}}) = \frac{\alpha+2}{2\eta^{\frac{2\alpha+2}{\alpha+2}}} \left(\frac{2}{2\alpha+3}\right)^{\frac{2\alpha+3}{\alpha+2}}. \quad (53)$$

VII. DESIGN ALGORITHM

At this point we know that the new mechanism is capable of trapping dipoles, but several conditions have to be fulfilled simultaneously. The following algorithm provides a systematic way for designing trap parameters that satisfy the various conditions.

1. We start with the stability criterion (32) and use the definition of β in (10) to obtain the condition

$$l_0 < \left[\frac{q_s(\eta) \alpha I \rho_0^\alpha}{M\eta} \right]^{1/2}. \quad (54)$$

Denote by D the desired location of the radial equilibrium distance of the trapped dipole. The size of D may depend on many factors, prime among them the spatial extent of the field-generating electrodes. If, e.g., the field is generated by a wire, we obviously need to choose $D > r_{\text{wire}}$, where r_{wire} is the radius of the wire. With D chosen, and

$$D = \rho_0 l_0, \quad (55)$$

we now have

$$\frac{1}{\rho_0^2} = \frac{l_0^2}{D^2} < \left[\frac{q_s(\eta) \alpha I}{MD^2} \right] \frac{\rho_0^\alpha}{\eta}. \quad (56)$$

With (19) this implies

$$\eta > \frac{2MD^2}{q_s(\eta) \alpha (\alpha+1) I}. \quad (57)$$

Since the right-hand side of (57), via $q_s(\eta)$, depends on η , we solve (57) iteratively. Starting with $q_s(\eta) = 0.9$, an η value satisfying (57) is usually obtained after only a few iterations of (57).

2. With η chosen, we may now use (55) to compute l_0 according to

$$l_0 = \frac{D}{\rho_0} = \frac{D}{\left(\frac{\alpha+1}{2}\right)^{\frac{1}{\alpha+2}} \eta^{\frac{2}{\alpha+2}}}. \quad (58)$$

Since η satisfies (57), l_0 , computed according to (58), automatically satisfies (54).

3. With η chosen and l_0 computed, we may now derive a condition for the drive frequency Ω . From (53) with (49) and (11), we obtain

$$\Omega > \left[\frac{8g}{(\alpha+2)l_0} \left(\frac{2\alpha+3}{2} \right)^{\frac{2\alpha+3}{\alpha+2}} \right]^{1/2} \eta^{\frac{\alpha+1}{\alpha+2}}. \quad (59)$$

4. With η , l_0 , and Ω known, we now use (12) to determine V_{dc} according to

$$V_{dc} = \frac{M\Omega^2 l_0^{\alpha+2}}{4\alpha\nu}. \quad (60)$$

5. With all design parameters chosen, we may now perform an important verification step, the numerical solution of the system of equations

$$\ddot{\rho} + [1 - 2\eta \cos(2\tau)] \frac{\cos(\theta)}{\rho^{\alpha+1}} - \gamma = 0, \quad (61)$$

$$\ddot{\theta} + \beta[1 - 2\eta \cos(2\tau)] \frac{\sin(\theta)}{\rho^\alpha} = 0, \quad (62)$$

i.e. the system (15), (16) including the effect of gravity in the radial equation. Only if the system (61), (62) exhibits stable solutions did we indeed construct a parameter set that leads to the stable trapping of point dipoles \mathbf{p} in the field \mathbf{E} . Failure of this verification step indicates that the trap parameters were chosen too close to the analytical estimates of the stability borders. Allowing for larger safety margins will cure the problem.

VIII. FERROELECTRIC RODS

Ferroelectric rods of mass M , trapped in the electric field of a metallic, spherical electrode of radius r_c , provide an illustration of the new trapping mechanism that may be realized experimentally. To be specific, we study the case of thin rods of barium titanate, a classic ferroelectric material [38] with a spontaneous polarization of $P_s = 0.15 \text{ Cm}^{-2}$ [39] and a density of 6 g/cm^3 [40]. The moment of inertia of thin, cylindrical rods is [41]

$$I = \frac{1}{12} M b^2, \quad (63)$$

where b is the length of the rods. We specify $b = 1 \text{ mm}$, $D = 2 \text{ mm}$, and $\nu = r_c = 1 \text{ mm}$. According to step 1 of the design algorithm and $q_s = 0.9$, we obtain $\eta > 17.8$. We choose $\eta = 25$, which satisfies (57). According to step 2 we obtain $l_0 = 0.36 \text{ mm}$. According to step 3 we obtain $\Omega > 7811 \text{ s}^{-1}$; we choose $\Omega = 1.5 \times 10^4 \text{ s}^{-1}$. Step 4, then, yields $V_{dc} = 18.9 \text{ V}$. The checks on β and γ yield $\beta = 0.78 < q_s \rho_0^2 / \eta = 1.1$ and $\gamma = 4.8 \times 10^{-4} < 2(2/7)^{7/4} / \eta^{3/2} = 1.8 \times 10^{-3}$. According to (20) the micro-motion amplitude of the rod is $\rho_1 l_0 = 26.6 \mu\text{m}$, which allows enough clearance for the rod to oscillate around $r = D$. The numerical check of stability according to step 5 was performed for $\eta = 25$, $\beta = 0.78$, $\alpha = 2$, and $\gamma = 4.8 \times 10^{-4}$ over a time interval of $\Delta\tau = 500\pi$ for the following $7^4 = 2401$ initial conditions: $(\rho(\tau = 0) = 5.3 + j \times 0.03, \dot{\rho}(\tau = 0) = k \times 0.003, \theta(\tau = 0) = l \times 0.01, \dot{\theta}(\tau = 0) = m \times 0.01)$, $j, k, l, m = -3, \dots, 3$. It was verified graphically that all 2401 trajectories are stable.

IX. DISCUSSION

The new ac/dc trapping mechanism proposed here is fundamentally different from the saddle-point mechanism employed for the successful demonstration of electrodynamic trapping of polar molecules [23, 24]. The trap proposed here makes use of *monopole* fields, i.e. particles are trapped in close proximity to *sources* of the electric field. In

addition, while the pseudo-potential of higher-multipole traps generates a *focusing* force, the pseudo-potential of the trap proposed here generates a *defocusing* force, which attempts to drive the particle toward $r = \infty$. Thus, the dc voltage is an essential ingredient for the trap discussed in this paper: the dc voltage generates the attractive force counterbalancing the defocusing effect of the ac electric field. Thus, the trap discussed here is akin to the dynamically stabilized inverted pendulum [42, 43], a classic lecture demonstration in introductory mechanics courses.

At a first glance, the new trap introduced here resembles a trap investigated several years ago by Riis and Barnett [44]. However, there are several important differences. (a) The Riis/Barnett trap aims to trap molecules in the ground state [44], whereas the new trap employs a dynamical trapping mechanism in the radial and angular degrees of freedom. Quantum mechanically, trapping in the angular degree of freedom corresponds to a wave function in which the trapped particle finds itself in an angularly localized wave packet that does not correspond to the rotational ground state of the trapped particle. (b) For the Riis/Barnett trap gravity is essential [44, 45], whereas the new trap works even without gravity (see Sec. V). (c) In contrast to the Riis/Barnett trap, which does not use a permanent dipole moment, a permanent dipole moment is *essential* for the new trap to work. (d) No stable trajectories have been found [45] for the Riis/Barnett trap. Far from being trivial, the reason why the Riis/Barnett trap does not work is interesting and instructive: The micro-motion in the Riis/Barnett trap is too large [45]. Contrary to the dynamics exhibited by the Riis/Barnett trap, the micro-motion in the new trap is very small (see Fig. 1), explaining why the new trap works. In our case, the small micro-motion (see Fig. 1) is the reason why the pseudo-potential method is valid and leads to stable trapping. The importance of a small micro-motion for stable trapping and for the validity of the pseudo-potential method was also pointed out by Cornell [46].

Our analysis did not include the possibility that the trapped dipoles may have orbital angular momentum, i.e., the possibility of revolving around the field-generating electrodes. Since orbital angular momentum is not an essential part of the trapping mechanism, like it is, e.g., in the classic Kingdon trap [11, 14, 15], this is not an essential omission. On the contrary: It is one of the strengths of the new trap that it works for zero orbital angular momentum. In fact, in the presence of a cooling mechanism, zero orbital angular momentum will be achieved automatically. Zero orbital angular momentum is a problem for traps that need orbital angular momentum to work (see, e.g., [20, 21]); it is not a problem for the new trap. It has been checked that the new trap does work in the presence of orbital angular momentum. Some aspects of this result are not surprising. In the case $\alpha = 2$, e.g., orbital angular momentum creates a centrifugal force with the same radial dependence as the dc electric force. Thus the effects of angular momentum do not structurally change the equations of motion and can be counterbalanced by an adjustment of ac and dc voltages. The fact that the orientation of the dipole on its trip around the electrode adiabatically follows a near-alignment with small oscillations around the orbital radius vector is more of a surprise. This mechanism, however, is not new; it forms the dynamical basis of the Sekatskii/Schmiedmayer trap [20, 21], which has already been demonstrated to work experimentally [47]. In fact, the Sekatskii/Schmiedmayer trap [20, 21] is a limiting case of the new trap in the presence of orbital angular momentum but zero ac electric field. Since the stabilizing repulsive force counteracting the attractive dc field is provided by orbital angular momentum for zero ac field, and by the repulsive pseudo-force for zero orbital angular momentum, a “chirping mechanism” may be envisioned: As the particle loses angular momentum due to cooling or damping, an ac voltage may be switched on, providing the repulsive force that keeps the trapped particle(s) from crashing into the electrode(s). The final state is then the zero orbital angular momentum state, fully stabilized by the ac field according to the new mechanism.

The trapping mechanism discussed here is also different from the mechanism of optical tweezers [48–50]. Optical tweezers work astonishingly well for small particles ranging from atoms and molecules to biological cells and even buoyant, small organisms [29, 49]. However, in contrast to the scheme proposed here, optical tweezers may not be able to hold a mm sized rod of ferroelectric against gravity, and the frequency of optical tweezers ($\sim 10^{15}$ Hz) is orders of magnitude larger than is required according to the new trapping scheme. Thus, differing in mechanism and range of application, each of these two mechanisms has its own optimal niche of applicability.

In our analysis above, we used $E \sim 1/r^\alpha$ and examples were presented for $\alpha = 2$. Inverse powers is a natural choice (wires, e.g., generate $\alpha = 1$; spheres generate $\alpha = 2$; oppositely charged spheres, e.g., generate $\alpha = 3$ for large r), but not necessary. Superpositions of such fields as well as many other field configurations may lead to stable trapping, provided the corresponding stability criteria are worked out and are satisfied.

For the time-dependent part of the electric field of the trap we chose a $\cos(\Omega t)$ drive (harmonic drive). This, again, is not essential. Any drive envelope, such as, e.g., rectangular or impulsive (“ δ kicks”), can be accommodated and may yield stable, trapped solutions following proper adjustment of the β , γ , and η criteria. Impulsive drives, in particular, offer the possibility of representing the dynamics of the dipole in the form of iterated mappings [31]. This considerably simplifies the analytical and numerical analysis of the trap.

Concerning the case of trapped barium titanate rods, we have to be careful that the applied electric fields do not exceed the coercive field strength, i.e. a field strength that, applied in the opposite direction, would result in a reversal of the direction of the permanent polarization of the rods. Since, according to (9), $V_{ac} = 2\eta V_{dc}$, and $V_{dc} = 18.9$ V in our example, the ac electric field at the position $D = 2$ mm is $E_{ac} = r_c V_{ac}/D^2 = 2400$ V/cm. Since typical coercive

fields for barium titanate are on the order of 10 kV/cm [51], the field in our example is tolerable. However, if actual experiments are contemplated, it may be advisable to optimize the trapping parameters and/or the nature of the trapped particles. Rods made of croconic acid crystals [52], e.g., may be easier to trap than the barium titanate rods discussed in Sec. VIII.

Another concern is the large dielectric constant of barium titanate, which may result in an appreciable induced dipole moment. At room temperature, ϵ_r , the relative dielectric constant, may reach values of $\epsilon_r \approx 5000$ [39]. In this case the induced polarization is $P_{\text{ind}} = \epsilon_0 \epsilon_r E_{\text{ac}} = 1.1 \times 10^{-4} \text{ C/m}^2 \ll P_s = 0.15 \text{ C/m}^2$, where ϵ_0 is the permittivity of the vacuum. We conclude that induced polarization is not an important effect. Even if for some trapped particle species this effect should be large, the induced polarization may be fully compensated for by adjusting V_{ac} and V_{dc} .

While this paper focuses on the case of a single stored dipole, we may also study the case of many, simultaneously stored dipoles. In the presence of a cooling mechanism, such as laser cooling [53] (for atomic-sized particles) or buffer-gas cooling [54] (for atomic-, nano-, and macroscopic-sized particles), trapped particle densities may become large enough that dipole-dipole interactions are important. In the case of molecules this may allow us to study new ferroelectric phases of dilute neutral (trapped) molecular gases. In the case of small ferroelectric particles, in analogy to the geometric arrangements of trapped Coulomb crystals [16–18], a geometrically ordered dipolar phase may be generated and studied. This may result in an interesting contribution to the emerging field of granular materials [55].

X. SUMMARY AND CONCLUSIONS

This paper presents a novel electrodynamic trap for the stable confinement of neutral particles with permanent electric dipole moments. The mechanism of the trap differs profoundly from currently demonstrated or proposed neutral-particle traps. While conventional electric traps are based on energy shifts in selected quantum states and employ higher-multipole fields as an essential ingredient of trapping, the new trap uses a superposition of *monopole* fields, i.e. an attractive, static dc electric field and an ac field, whose net effect results in strong repulsion. If certain conditions on the strengths of the dc and ac fields are met, stable trapping results at the point where attractive and repulsive forces are in equilibrium. A mechanical analogue of this trapping mechanism is the dynamically stabilized inverted pendulum. Stability of the trap is proved with the help of an analytical stability analysis, supplemented with detailed numerical molecular trajectory simulations. The effect of gravity is considered and included. The example of thin barium titanate rods indicates that the trap works in practice. It is possible that the trap also works for polar (macro) molecules. Although there are no magnetic charges, and magnetic fields are divergence-free, it is possible that close to a magnetic pole as a field generating “source” a superposition of static and oscillating magnetic fields may result in a magnetic analog of the trapping mechanism discussed here.

-
- [1] H. G. Dehmelt, in *Advances in Laser Spectroscopy* (edited by F. T. Arecchi, F. Strumia, and H. Walther), 153–187 (Plenum, NY, 1983).
 - [2] D. J. Wineland, W. M. Itano, and R. S. Van Dyck, in *Adv. Atom. Molec. Phys.*, Vol. **19** (edited by D. R. Bates and B. Bederson), 135–186 (Academic, NY, 1983).
 - [3] D. J. Wineland and W. M. Itano, *Phys. Lett.* **82A**, 75 (1981).
 - [4] H. G. Dehmelt, *IEEE Trans. Instrum. Meas.* **IM-31**, 83 (1982).
 - [5] M. Amoretti *et al.*, *Nature* **419**, 456 (2002).
 - [6] J. N. Tan *et al.*, *Nucl. Instr. Meth. Phys. Res. B* **214**, 22 (2004).
 - [7] M. H. Anderson, J. R. Ensher, M. R. Matthews, C. E. Wieman, and E.A. Cornell, *Science* **269**, 198 (1995).
 - [8] K.B. Davis, M.O. Mewes, M.R. Andrews, N.J. van Druten, D.S. Durfee, D.M. Kurn, and W. Ketterle, *Phys. Rev. Lett.* **75**, 3969 (1995).
 - [9] *Quantum Information Processing*, edited by G. Leuchs and Th. Beth (Wiley-VCH, Weinheim, 2003).
 - [10] M. Tsuchiya and H. Ohsaki, *IEEE Transactions on Magnetics* **36**, 3683 (2000).
 - [11] K. H. Kingdon, *Phys. Rev.* **21**, 408 (1923).
 - [12] F. M. Penning, *Physica* **3**, 873 (1936).
 - [13] W. Paul, O. Osberghaus, and E. Fischer, *Forschungsber. Wirtsch. Verkehrsminist. Nordrhein-Westfalen* **415**, 1 (1958).
 - [14] T. Biewer, D. Alexander, S. Robertson, and B. Walch, *Am. J. Phys.* **62**, 821 (1994).
 - [15] D. A. Church, *Phys. Rep.* **228**, 253 (1993).
 - [16] F. Diedrich, E. Peik, J. M. Chen, W. Quint, and H. Walther, *Phys. Rev. Lett.* **59**, 2931 (1987).
 - [17] D. J. Wineland, J. C. Bergquist, W. M. Itano, J. J. Bollinger, and C. H. Manney, *Phys. Rev. Lett.* **59**, 2935 (1987).
 - [18] R. Blümel, J. M. Chen, E. Peik, W. Quint, W. Schleich, Y. R. Shen, and H. Walther, *Nature* **334**, 309 (1988).
 - [19] W. H. Wing, *Phys. Rev. Lett.* **45**, 631 (1980).
 - [20] S. K. Sekatskii, *JETP Lett.* **62**, 916 (1995).

- [21] S. K. Sekatskii and J. Schmiedmayer, *Europhys. Lett.* **36**, 407 (1996).
- [22] H. L. Bethlem, G. Berden, F. M. H. Crompvoets, R. T. Jongma, A. J. A. van Roij, and G. Meijer, *Nature* **406**, 491 (2000).
- [23] J. van Veldhoven, H. L. Bethlem, and G. Meijer, *Phys. Rev. Lett.* **94**, 083001 (2005).
- [24] H. L. Bethlem, J. van Veldhoven, M. Schnell, and G. Meijer, *Phys. Rev. A* **74**, 063403 (2006).
- [25] D. DeMillea, D.R. Glenn, and J. Petricka, *Eur. Phys. J. D* **31**, 375 (2004).
- [26] R. V. E. Lovelace, C. Mehanian, T. J. Tommila, and D. M. Lee, *Nature* **318**, 30 (1985).
- [27] A. L. Migdall, J. V. Prodan, W. D. Phillips, T. H. Bergeman, and H. J. Metcalf, *Phys. Rev. Lett.* **54**, 2596 (1985).
- [28] K. C. Neuman, E. H. Chadd, G. F. Liou, K. Bergman, and S. M. Block, *Biophys. J.* **77**, 2856 (1999).
- [29] A. Ashkin and J. M. Dziedzic, *Science* **235**, 1517 (1987).
- [30] L. D. Landau and E. M. Lifshitz, *Mechanics* (Pergamon, Oxford, 1960).
- [31] E. Ott, *Chaos in Dynamical Systems* (Cambridge University Press, Cambridge, 1993).
- [32] M. Abramowitz and I. A. Stegun, *Handbook of Mathematical Functions* (National Bureau of Standards, Washington DC, 1964).
- [33] H. G. Dehmelt, *Adv. Atom. Mol. Phys.* **3**, 53 (1967).
- [34] H. Friedrich, *Theoretical Atomic Physics*, third edition (Springer, Berlin, 2006).
- [35] B. M. Lamb and G. J. Morales, *Phys. Fluids* **26**, 3488 (1983).
- [36] R. Blümel, *Phys. Rev. A* **51**, R30 (1995).
- [37] I. Garrick-Bethell, Th. Clausen, and R. Blümel, *Phys. Rev. E* **69**, 056222 (2004).
- [38] C. Kittel, *Introduction to Solid State Physics* (John Wiley & Sons, New York, 1971), p. 476.
- [39] W. J. Merz, *Phys. Rev.* **76**, 1221 (1949).
- [40] *Handbook of Chemistry and Physics*, 55th Edition, 1974–1975, edited by R. C. Weast (CRC Press, 1974), p. B-72.
- [41] J. B. Marion and S. T. Thornton, *Classical Dynamics*, third edition (Harcourt Brace Jovanovich, Fort Worth, 1988).
- [42] J. G. Fenn, D. A. Bayne, and B. D. Sinclair, *Am. J. Phys.* **66**, 981 (1998).
- [43] E. I. Butikov, *Am. J. Phys.* **69**, 755 (2001).
- [44] E. Riis and S. M. Barnett, *Europhys. Lett.* **21**, 533 (1993).
- [45] E. Riis and S. M. Barnett, *Europhys. Lett.* **30**, 441 (1995).
- [46] E. A. Cornell, *Europhys. Lett.* **30**, 439 (1995).
- [47] H. J. Loesch and B. Scheel, *Phys. Rev. Lett.* **85**, 2709 (2000).
- [48] A. Ashkin, J.M. Dziedzic, J.E. Bjorkholm, and S. Chu, *Opt. Lett.* **11** 288 (1986).
- [49] S. Chu, *Sci. Am.* **266**, 70 (February, 1992).
- [50] S. M. Block, *Nature* **360**, 493 (1992).
- [51] J. K. Hulm, *Nature* **160**, 127 (1947).
- [52] S. Horiuchi, Y. Tokunaga, G. Giovannetti, S. Picozzi, H. Itoh, R. Shimano, R. Kumai, and Y. Tokura, *Nature* **463**, 789 (2010).
- [53] S. Stenholm, *Rev. Mod. Phys.* **58**, 699 (1986).
- [54] R. V. Krems, D. Zgid, G. Chalasinski, J. Klos, and A. Dalgarno, *Phys. Rev. A* **66**, 030702(R) (2002).
- [55] A. Mehta, *Granular Matter: An Interdisciplinary Approach* (Springer, New York, 1994).